

Evaluation of the splitting tension test for concrete from a fracture mechanical point of view

V. Malárics & H.S. Müller

Krlsruhe Institute of Technology (KIT), Germany

ABSTRACT: The presented work aimed at the derivation of a consistent conversion formula between the splitting tensile strength $f_{ct,sp}$ and the uniaxial tensile strength f_{ct} for the entire spectrum of structural concretes used in practice. First, the validity of the splitting tension test had to be verified. To achieve this, an extensive experimental programme was carried out. Furthermore, a testing method was developed to detect the cracking sequence in the specimen during the splitting tension tests. Based on fracture mechanical parameters obtained by the experiments, the splitting tension test was analyzed by means of numerical simulations as well. To investigate the interdependency of the compressive strength and the splitting and uniaxial tensile strength, concretes of different strength classes were tested. Both experimental and numerical test results show a complex failure mechanism in the specimen during the splitting tension test.

1 INTRODUCTION

The tensile strength of concrete is a very important parameter in the design of civil engineering structures. In order to determine the tensile strength of concrete for existing structures, experiments are necessary. Because of the complex nature of uniaxial tension tests, usually splitting tension tests are carried out on cylindrical specimens or cores.

The splitting tensile strength $f_{ct,sp}$ can be calculated by a formula, which was derived from the theory of elasticity (see Equation 1):

$$f_{ct,sp} = \frac{2 \cdot F_u}{\pi \cdot D \cdot L} \quad (1)$$

where $f_{ct,sp}$ = splitting tensile strength [MPa], F_u = measured peak load [N], D = diameter of specimen [mm] and L = length of specimen [mm] (see Fig. 1).

Due to the differences between the assumed boundary conditions and the true test set-up – such as a deviant material behaviour and differences in the loading of the specimen – various authors question the applicability of splitting tension test for estimating the uniaxial tensile strength f_{ct} (e.g. Castro-Montero et al. (1995), Hannant et al. (1973) and Tedesco et al. (1993)).

Castro-Montero et al. (1995) analysed the fracture mechanism of specimens during splitting tension tests by laser holographic interferometry. They found that the first cracks opened while reaching approx. 70 % of the peak load. However, they did not initiate in the centre of the specimens cross section – where according to the theory of elasticity the tensile stresses should have a maximum – but in the

loading plane (see Fig. 1), approximately at a third of the height of the specimen in conjunction with a wedge rupture below the load bearing strips resulting from a secondary cracking. Castro-Montero et al. also detected a strong dependency between the fracture processes of the splitting tension specimen and the geometry and test set-up, respectively.

The experiments of Tedesco et al. (1993) and Hannant et al. (1973) showed an identical failure mechanism. In order to study the dependency of the splitting tensile strength on the biaxial compression state of stress in the area below the load bearing strips, Hannant et al. also tested specimens consisting of two half-shells, which were casted separately.

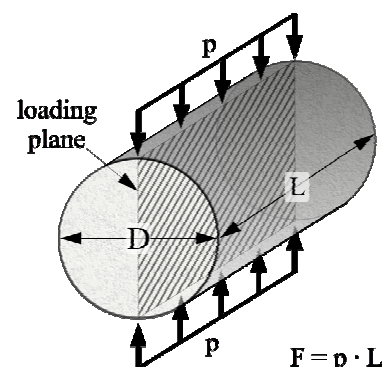


Figure 1. Schematic picture of the loading of the specimen in a splitting tension test.

This way, no tensile stresses could occur in the loading plane of the specimen during the splitting tension tests.

The obtained splitting tensile strength was 75 % of the value measured on specimens of cylindrical geometry. The fracture images of both sorts of specimen did not show any noteworthy differences. Consequently Hannant et al. suggested that the main part of the applied load is required to develop the wedge rupture below the load bearing strips. Hence as only a minor part of the applied load induces the tensile stresses in the loading plane of the specimen, the validity of Equation 1 to calculate the splitting tensile strength can be questioned.

However, the conclusions of the mentioned authors are solely based on single test series. In order to clarify the validity of the splitting tension test for the entire spectrum of structural concrete strengths used in practice, an extensive experimental and numerical programme was carried out. Based on the results of these, conversion formulae between the splitting tensile strength $f_{ct,sp}$ and the uniaxial tensile strength f_{ct} were derived.

2 EXPERIMENTAL INVESTIGATIONS

2.1 Experimental programme, preparation of specimens, test set-up

In order to obtain data for the derivation of a conversion formula, experiments consisting of compression, splitting and uniaxial tension tests were carried out. The comprehensive experimental programme incorporated three normal strength concretes (NSC-1, NSC-2 and NSC-3) as well as two high strength concretes (HSC-1 and HSC-2) each with different aggregates (gravel and crushed aggregates).

To classify the concretes, the compressive strength f_c was determined on cubes ($f_{cm,cube}$) with an edge length of 150 mm and on cylinders (f_{cm}) with a diameter D of 150 mm and a length L of 300 mm.

The splitting tension tests were performed on cylinders with varying geometries and concreting methods. On site, the characteristic values of existing concrete structures can only be determined by taking core samples. Therefore, cores with $D/L = 150/300$ mm and $D/L = 75/150$ mm were used (see Fig. 2). Moreover, specimens with $D/L = 150/300$ mm, cast in accordance with DIN EN 12390-6 (2001) in cylindrical formworks, were tested (see Fig. 2).

Furthermore, in order to detect the cracking sequence splitting tension tests on specimens with $D/L = 150/300$ mm, $D/L = 150/75$ mm and $D/L = 300/150$ mm were carried out (see Fig. 2). For these series a normal strength (NSC_{G-3}) and a high strength concrete (HSC_{G-1}), respectively with gravel aggregate were used.

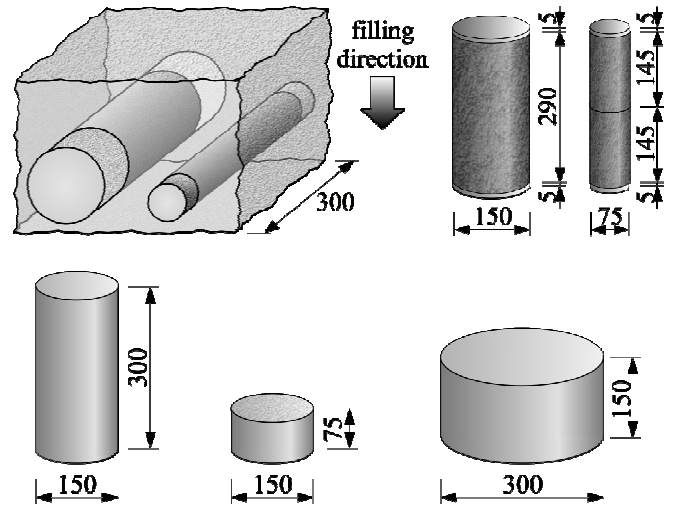


Figure 2. Geometry of specimens for the splitting tension test: cores (above) and prepared in formwork (below); dimensions in [mm].

For the uniaxial tension tests, specimens with different prism and core geometries were chosen. The concrete tensile strength f_{ct} , the tangent modulus of elasticity E_{c0} as well as the ultimate strain ϵ_c were determined on dog-bone shaped prisms (see Fig. 3 above). In order to record the complete stress-deformation relation, notched prisms were used (see Fig. 3 below). With notches sawed 20 mm in depth and 5 mm in width in the middle of the test specimens, the resulting cross section corresponded to the cross section of the dog-bone shaped prisms (100×60 mm²).

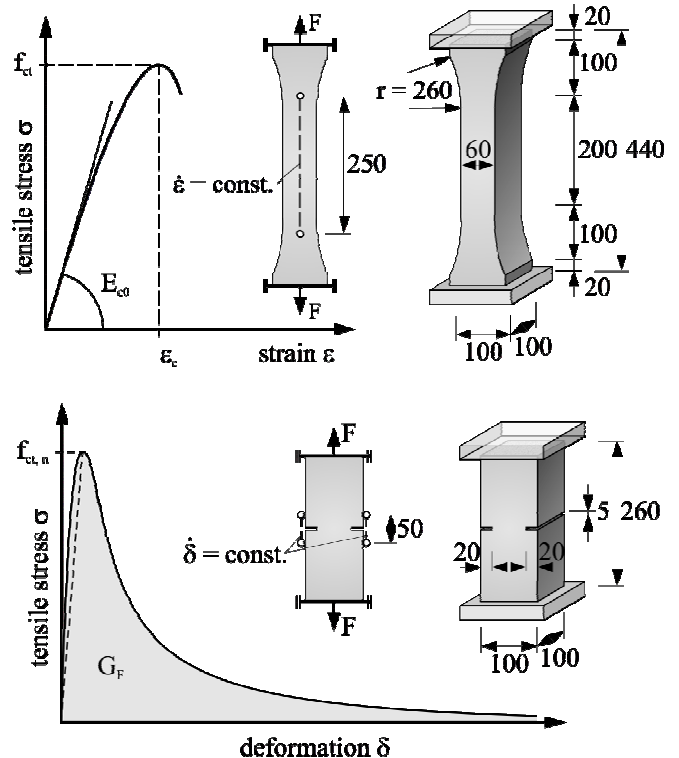


Figure 3. Geometry of unnotched dog-bone shaped prisms (above) and notched prisms (below) with illustration of the typical gradient progression and indication of characteristic concrete properties; dimensions in [mm].

All specimens were un moulded at the age of 1 day and then stored at a relative humidity of at least 95 % and an air temperature of 20 °C (DIN EN 12390: 2001). The cores were taken from concrete walls elements (see Fig. 2, above) at the age of approx. 1 week and subsequently stored as mentioned above. The specimens for tension tests were sealed 24 hours before testing with a thin polyethylene foil and their front surfaces were coated with epoxy resin. All tests were carried out at a concrete age of 28 days.

The testing of splitting tensile strength $f_{ct,sp}$ was accomplished without interlayers, using a centring device, according to DIN EN 12390-6 (2001) (see Fig. 4). Thus, both the centric specimen installation and the load application along parallel surface lines of the core could be ensured. This method had to be used because preliminary tests had revealed that high strength specimens (C80/95 and higher) could drop out of the testing machine due to early failure of the hard masonite plates that would have had to be used according to DIN EN 12390 (2001).

In order to obtain the cracking sequence in the specimens during the splitting tension tests on the face side of the specimens conducting silver varnish stripes were applied (see Fig. 5). If a crack developed, the very brittle stripes were immediately broken, interrupting the electric circuit. The voltage signals were detected depending on the geometry of the specimen using 7 (D/L = 150/300 and D/L = 150/75 mm) and 14 (D/L = 300/150 mm) channels by a measuring amplifier with a detection rate of 1 MHz.

Simultaneously the tests were documented with a high-speed camera (SpeedCam Visario, 10000 picture/s). With this set-up one channel of the measuring amplifier could be used as a trigger to start the camera recording just in time to register the whole cracking process.

In order to assure a uniform stress distribution over the whole cross section during uniaxial tension testing, rigid steel plates with a thickness of 35 mm were glued to both face sides of the tension specimens.

The tests were performed with non-rotatable boundaries on dog-bone shaped prisms with a strain rate

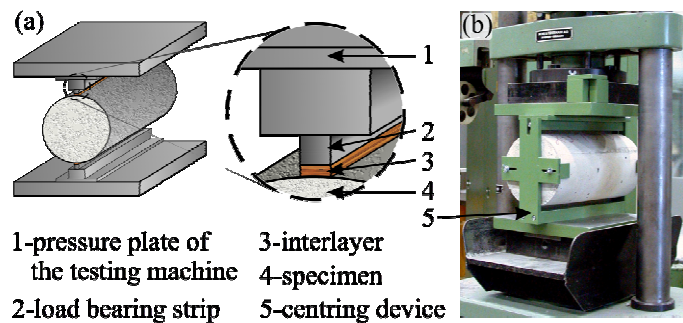


Figure 4. Schematic picture of the splitting tension test set-up according to DIN EN 12390-6 (2001) (a) and photo of the centring device, a specimen with D/L = 150/300 mm and the testing machine (b).

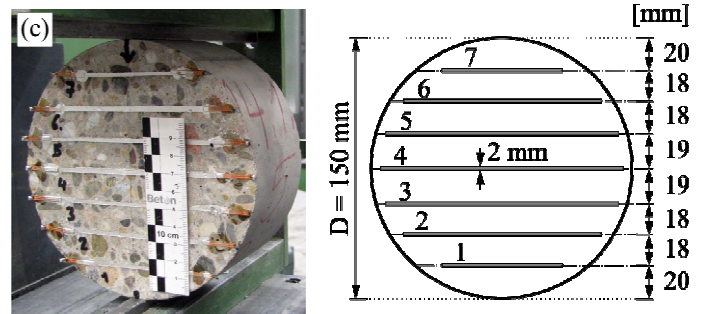
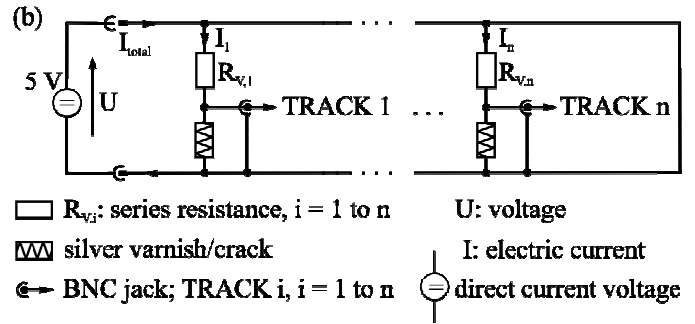
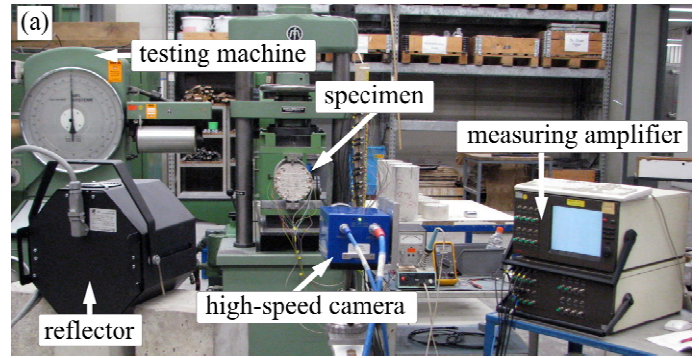


Figure 5. Set-up of the splitting tension test on a specimen with applied silver varnish stripes (a), testing scheme (b) and arrangement of the silver varnish stripes (c) for a specimen D/L = 150/75 mm.

of $\dot{\epsilon} = 0.06$ %/min and notched prisms with a deformation rate of $\dot{\delta} = 3 \cdot 10^{-2}$ mm/min. In contrast, the cores were tested with rotatable boundaries and a load application rate of 0.05 N/mm²·s in accordance with DIN 1048 (1991) and RILEM CPC7 (1975).

2.2 Results of experimental investigations

This chapter is limited to results with regard to the cracking sequences in the specimens during the splitting tension tests. Results of further test series are given in Malárics & Müller (2007) and are described in detail in Malárics (2010). In the following the observations presented are based on the results of four single measurements in each testing series. The mean values of the concrete characteristics are given in Table 1. The standard deviations are denoted in parentheses.

The failure mechanism of specimens with D/L = 150/300 mm using normal strength concrete with gravel (NSC_{G-3}) is shown in Figure 6. The results

Table 1. Material characteristics of the concretes, which were used in the splitting tension tests to detect the cracking sequence in the specimens; (standard deviation).

material parameter	D/L [mm/mm]	NSC _{G-3}	HSC _{G-2}
$f_{cm,cube}$ [MPa]	-	42 (0.9)	100 (3.6)
$f_{ct,sp}$ [MPa]	150/300	2.6 (0.02)	4.0 (0.51)
$f_{ct,sp}$ [MPa]	150/75	3.1 (0.08)	5.9 (0.22)
$f_{ct,sp}$ [MPa]	300/150	2.6 (0.30)	4.6 (0.43)

for high strength concrete with gravel (HSC_{G-2}) are depicted in Figure 7.

All findings show differences from the theoretical assumptions according to the theory of elasticity, as the first cracks did not occur in the centre point of the specimens cross section. Cracking was initiated on the face side of specimens with D/L = 150/300 mm for normal strength concretes approximately at a fourth of the height (see Fig. 6) and for high strength

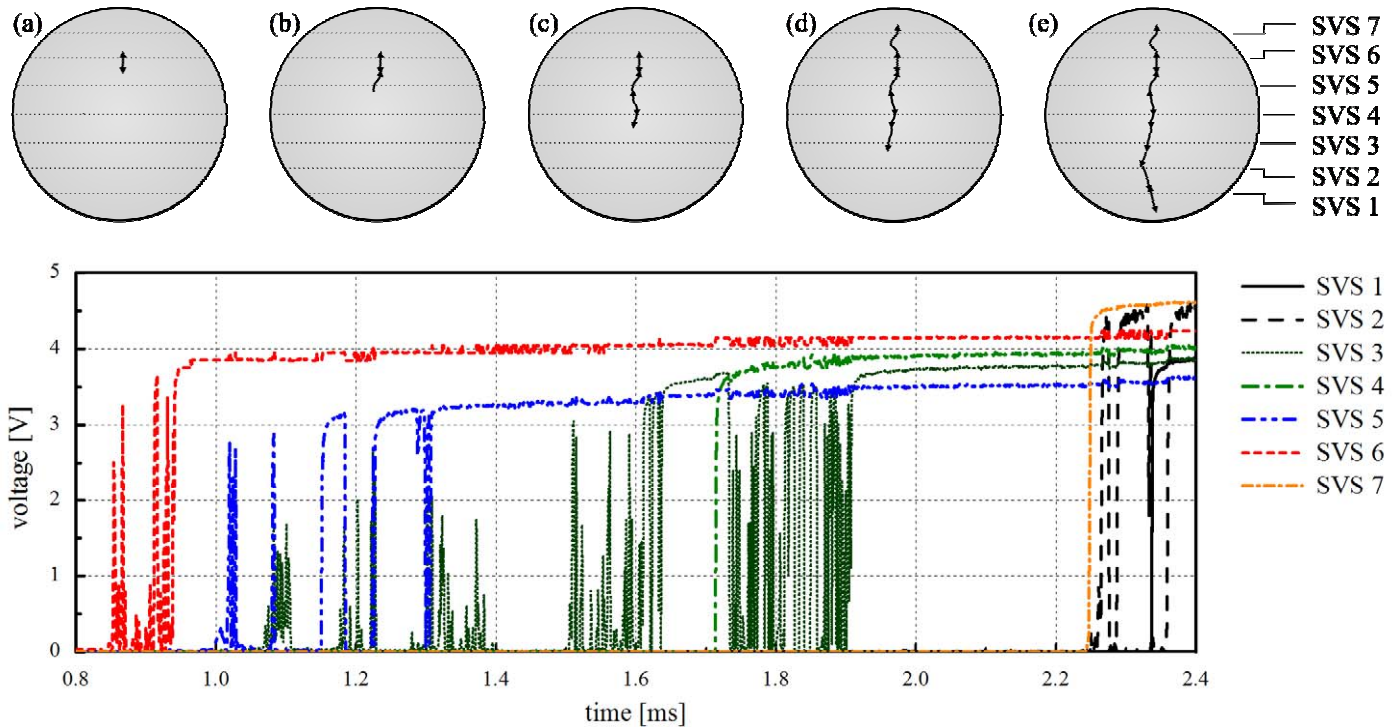


Figure 6. Cracking sequence in a splitting tension specimen with D/L = 150/300 mm for normal strength concrete NSC_{G-3}. Pictures of the high-speed camera (above) and results of the conduction measurement using silver varnish stripes (SVS) (below).

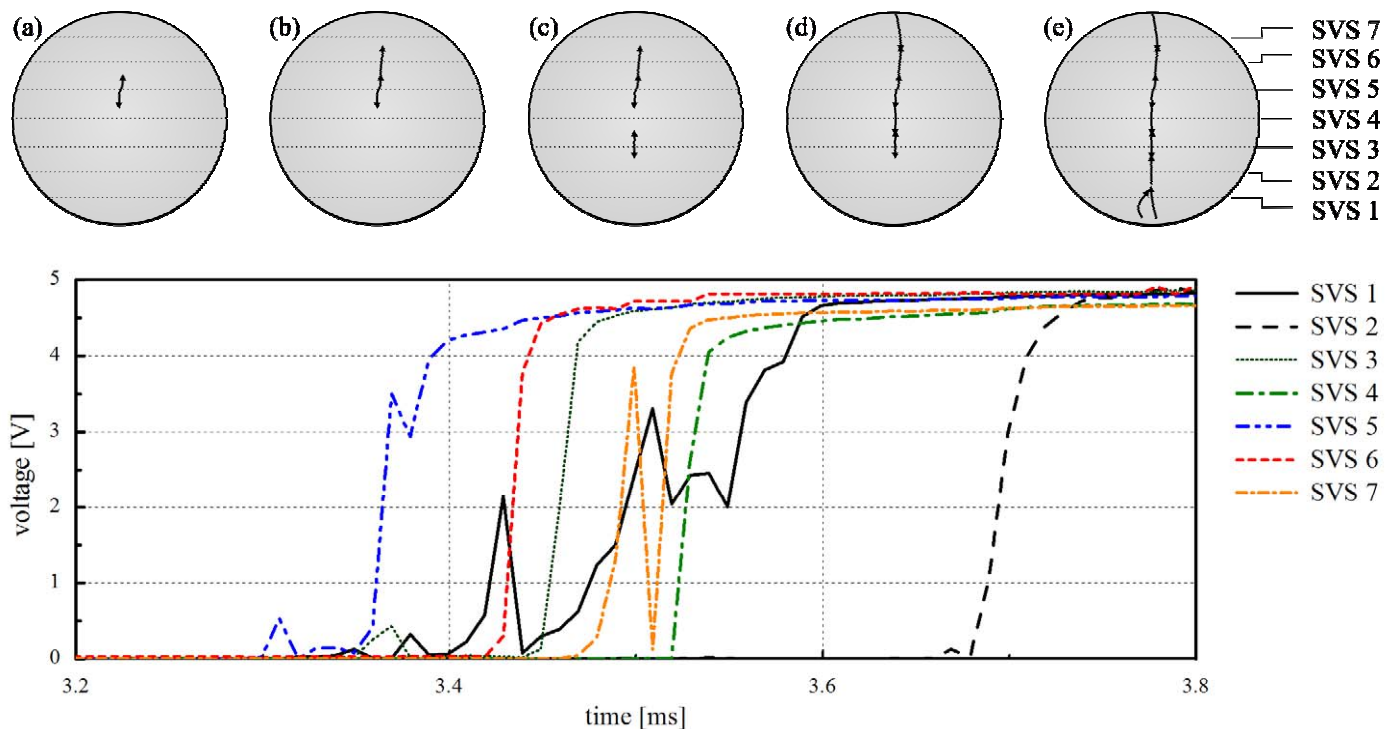


Figure 7. Cracking sequence in a splitting tension specimen with D/L = 150/300 mm for high strength concrete HSC_{G-2}. Pictures of the high-speed camera (above) and results of the conduction measurement using silver varnish stripes (SVS) (below).

concretes (see Fig. 7) approximately at a third of the height of the cross section. The pictures of the high-speed camera correspond with the detected signals of the conductivity measurements (compare Fig. 6 & Fig. 7 above and below, respectively). Because of their brittle material behaviour specimens made from high strength concrete showed considerably shorter failure durations of approx. 0.5 ms and less signal noise than the ones made from normal strength concretes (1.6 ms, compare Fig. 6 & Fig. 7 below).

In summary, the observations of the crack sequence in the splitting tension test revealed that the position where cracks initiate move towards the centre of the specimen if the concrete used is of higher strength and if the length of the specimen decreases, respectively. Furthermore in this case the failure duration decreases. Simultaneously the rupture line becomes straighter.

3 NUMERICAL INVESTIGATIONS

3.1 Simulations

The numerical simulations were carried out using the finite element code DIANA (2007). In order to ensure a realistic simulation of crack initiation and propagation, the cohesive crack model was employed. The "Crack Band Model" by Bažant, Z.P. & Oh, B.H. (1983) was selected and combined with the so-called "Fixed Crack Concept" to consider the direction of cracking (DIANA 2007). According to this concept, the direction of an initiated crack within an element remains fixed during the entire crack expansion. This concept has the advantage that inactive cracks, which opened in an earlier "load step" and closed again afterwards, can be reactivated.

The employed material parameters for the FE computation (see Table 2) were set according to the results of the experimental investigations. The heterogeneity of the concrete was considered by varying the uniaxial tensile strength f_{ct} assigned to the FE-elements according to Mechtcherine (2000).

Parameter combinations for the splitting tension test simulations resulted from the three different load bearing strip widths $b = 5, 10$ and 20 mm, the five concrete material parameter combinations A, B, C, D and E (see Table 3) and the cylinder diameters

Table 2. Overview of material parameter combinations for the numerical simulations.

material parameter combination	A	B	C	D	E
f_{cm} [MPa]	20	30	50	90	110
f_{ct} [MPa]	2.5	2.5	3.6	4.9	5.6
E_c [MPa]	28,000	28,000	32,000	40,000	45,000
G_F [N/m]	90	95	130	150	170
Poisson's n. [-]	0.2	0.2	0.2	0.2	0.2

Table 3. Overview of parameter combinations for the simulation of the splitting tension tests.

Parameter	value/combination
D [mm]	75, 150, 300
L [mm]	75, 150, 300
load bearing strip width b [mm]	5, 10, 20
interlayer	hard masonite
FE-element length l_{el} [mm]	1.785, 3.75, 7.5
material combination	A, B, C, D, E

tested ($D = 75, 150$ and 300 mm and $L = 75, 150$, and 300 mm). For all cylinder geometries, the proportion of mesh refinement and sample dimensions was held constant and was set proportional to the geometry as well. In the area of load introduction and in the centre line of the specimen, a mesh with square elements of uniform size was discretised (see Fig. 8). Special interface elements, so-called contact elements were used to simulate the contact in between the load bearing strips and the specimen. The use of these contact elements allowed for a separate discretisation of the FE-meshes for the load bearing strips and the specimen as well (see Fig. 8, detail 1 & 3).

The loading was applied as defined displacement of $\Delta u = 0.01$ mm. Preliminary simulations showed that this way a significantly more stable analysis and thus a longer convergence can be realized in comparison with calculations, in which the loading was applied as a force.

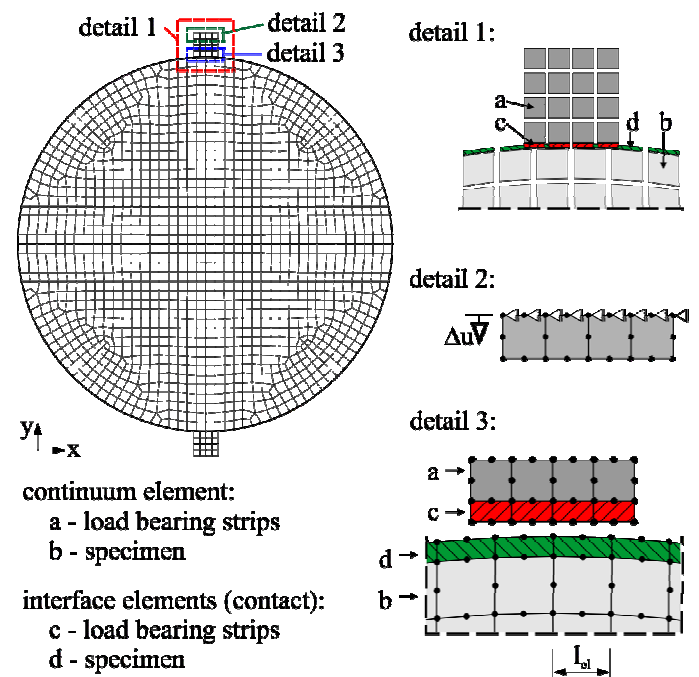


Figure 8. FE-models for the simulation of the splitting tension test: $D = 150$ mm, $b = 10$ mm and $l_{el} = 3.75$ mm.

3.2 Results of the numerical simulations

The verification of the numerical model by means of the experimental results of the splitting tension test, which were carried out on specimens with $D/L = 150/300$ mm, with load bearing strips made of steel

and with a width of $b = 10$ mm showed excellent results.

In the following the observations of simulations under the above mentioned boundary conditions will be outlined. Further results are particularised in Malárics (2010).

In order to illustrate the fracture mechanism in the model the crack strains in the cracked elements are depicted via colour scale. The crack propagation is given by a series of four pictures (see Fig. 9, below a & d). As the load-deformation diagram indicates, these images illustrate the corresponding cracks in the FE-model for different load cases (see Fig. 9, above). In order to point out the dependency

between the cracking and the strength of the concrete, the results of concretes A, C and E were chosen. Crack initiation starts independently of the concrete strength in the area beneath the load bearing strips where compressive stress prevails. The cracks then combine and propagate towards the centre of the cross section (see Fig. 9, below a & b). This phenomenon was also observed during the experiments. Moreover, the largest crack strains occurred in the simulations between the third and fourth of the model height, which also agrees with the findings of the cracking sequence detection method for the splitting tension test.

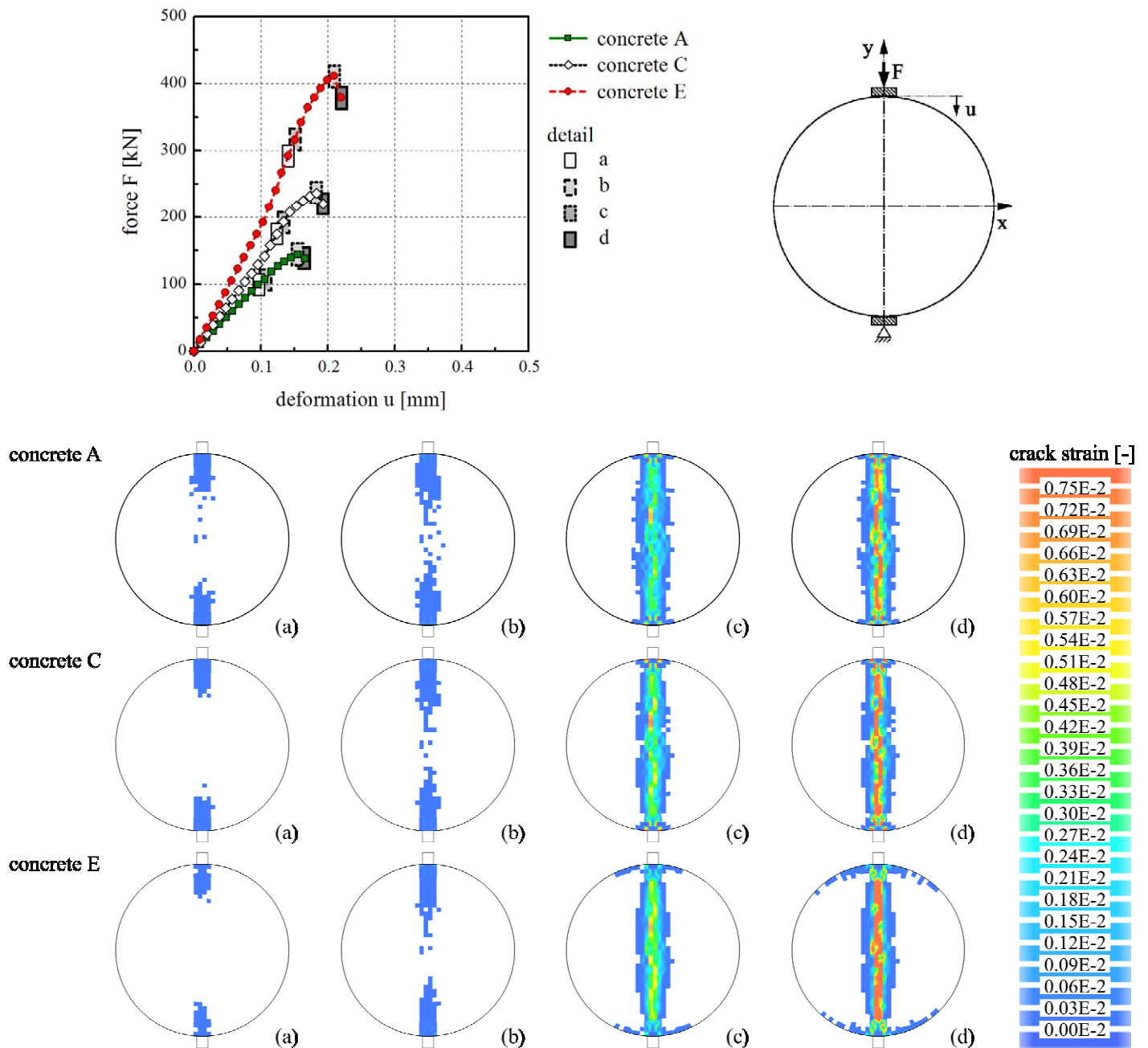


Figure 9. Load-deformation diagram (above) and crack propagation in the FE-model. Parameters: $D/L = 150/300$ mm, load bearing strip width $b = 10$ mm, $l_{cl} = 3.75$ mm.

Using an interlayer made of hard masonite led in the calculations to an increased splitting tensile strength of about 5 to 10 % in comparison with the ones calculated without an interlayer. Furthermore, the first cracks were not initiated beneath the load bearing strips but deeper within the cross section. In addition, the numerical results showed a size-effect for constant mesh density. With increasing sample dimensions, the calculated values of splitting tensile strength decrease.

4 CONVERSION FORMULA BETWEEN THE UNIAXIAL TENSILE STRENGTH AND THE SPLITTING TENSILE STRENGTH

Figure 10 represents the relation between the mean cylinder compressive strength f_{cm} and the ratio A of the mean uniaxial tensile strength f_{ctm} to the mean splitting tensile strength $f_{ctm,sp}$ for different kinds of specimens. Values for f_{ctm} were determined on dog-bone shaped prisms whereas data for $f_{ctm,sp}$ were obtained from cylinders and cores of different geometries. The ratio A shows a strong dependency on the specimen geometry and the concrete used. Moreover, it is obvious that the conversion factor proposed in CEB-FIP Model Code 90 (1993) is only valid for the ratio A , which was derived using the values of the splitting tensile strength obtained on cores with $D/L = 75/150$ mm. In every other case, it underestimates the ratio A for all concrete strengths which were investigated.

The main objective was to determine conversion formulae with simple mathematical formulations, which are manageable in practical situations. All the following conversion formulae were derived with the help of statistical methods and on the basis of the extended experimental data. In the following only the final results will be shown. The methodology is described in detail in Malárics (2010).

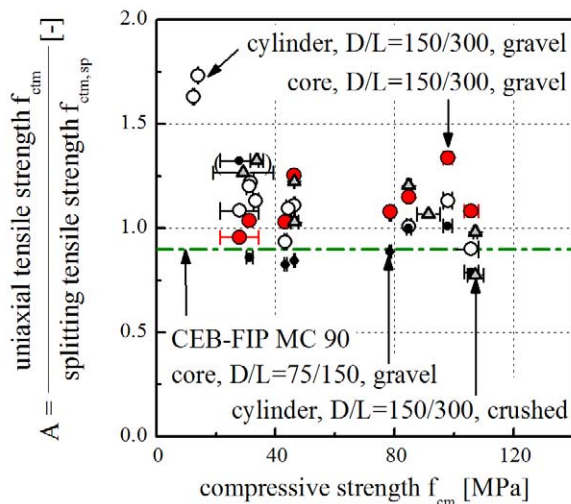


Figure 10. Comparison between the experimental results and the conversion factor proposed in CEB-FIP Model Code 90 (1993).

Based on the obtained findings in both extensive experimental and numerical programmes, it was not possible to generally determine the relationship between the uniaxial tensile strength and the splitting tensile strength with only one formula.

Figure 11 illustrates the derived relationships between the uniaxial tensile strength and the splitting tensile strength. These relationships for cylinder splitting tensile specimens consisting of concrete with both gravel and crushed aggregates can be described mathematically with the help of power functions according to Equations 2 and 5 (see Table 4). In comparison with the conversion factor proposed in CEB-FIP Model Code 90 (1993) the above mentioned new functions estimate higher values for the uniaxial tensile strength, especially for related splitting tensile strengths between $f_{ctm,sp} = 2$ and 5 MPa. Only, if the splitting tensile strength is determined on cores the conversion factor A is independent of the concrete compressive strength (see Eq. 3 & 4 in Table 4).

Applying a constant conversion factor for casted specimens, however, yields to wrong results, as

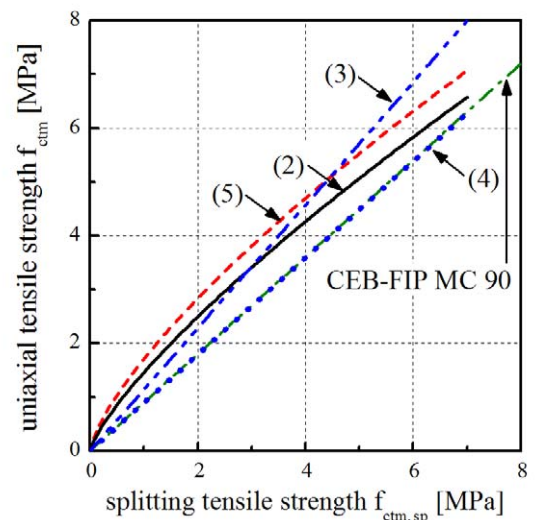


Figure 11. Comparison of the derived relationships between the uniaxial tensile strength and the splitting tensile strength. Both the specification and the functions of the curves are given in Table 4.

Table 4. Conversion formulae between the uniaxial tensile strength and the splitting tensile strength.

specimen property	D/L [mm/mm]	concrete aggregate	conversion formula	Eq. No.
cylinder	150/300	gravel	$f_{ct,m} = 1.46 \cdot f_{ctm,sp}^{0.77}$	(2)
core	150/300	gravel	$f_{ct,m} = 1.14 \cdot f_{ctm,sp}$	(3)
core	75/150	gravel	$f_{ct,m} = 0.90 \cdot f_{ctm,sp}$	(4)
cylinder	150/300	crushed	$f_{ct,m} = 1.71 \cdot f_{ctm,sp}^{0.73}$	(5)

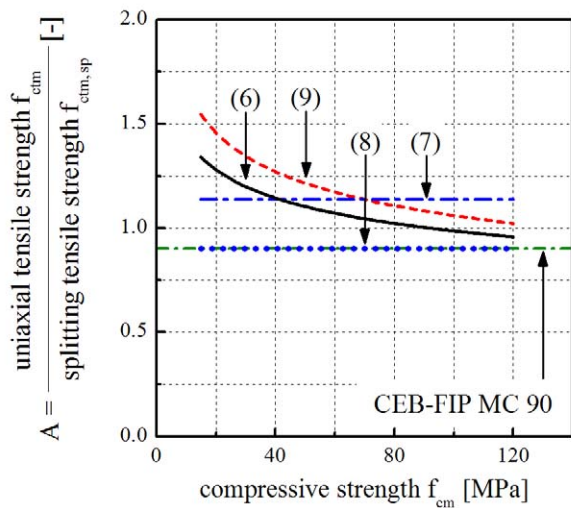


Figure 12. Comparison of the derived relationships between uniaxial tensile strength and splitting tensile strength based on the cylinder compressive strength. Both the specification and the functions of the curves are given in Table 5.

Table 5. Conversion formulae between the uniaxial tensile strength and the splitting tensile strength based on the compressive strength.

specimen property	D/L [mm/mm]	concrete aggregate	conversion formula	Eq. No.
cylinder	150/300	gravel	$A = 2.08 \cdot f_{cm}^{-0.16}$	(6)
core	150/300	gravel	$A = 1.14 \cdot f_{cm}$	(7)
core	75/150	gravel	$A = 0.90 \cdot f_{cm}$	(8)
cylinder	150/300	crushed	$A = 2.64 \cdot f_{cm}^{-0.20}$	(9)

A is a function of the concrete compressive strength. As can be seen from Figure 12, the factor A lies between 1.3 and 1.1 for normal strength concrete, but is approximately 1.0 for high strength concrete. Using the same geometry but with concrete consisting of crushed aggregates leads to values for A between 1.5 and 1.0 within the investigated strength range.

5 CONCLUSION

Both experimental and numerical investigations revealed a complex fracture mechanism in the specimens during the splitting tension tests. According to these findings not only the cracking itself but also the location of the crack initiation are affected by the concrete strength, specimen geometry and test set up. These observations are in conflict to the theory of elasticity, which forms the basis of the calculation formula for the splitting tensile strength applied today (see Eq. 1). Moreover, the relationship between the uniaxial tensile strength and the splitting tensile strength showed a significant dependency on the above mentioned parameters. The conversion factor of 0.9, which is proposed in CEB-FIP Model Code 90 (1993), is

not valid for all possible splitting tensile specimen geometries or concretes.

Based on the extended experimental results conversion formulae between the uniaxial tensile strength and the splitting tensile strength were derived both in a direct way and also dependent on the compressive strength. These relationships are valid, if the splitting tensile strength was obtained on specimens with $D/L = 150/300$ mm and on cores with $D/L = 150/300$ mm and $D/L = 75/150$ mm. The mathematical formulation of the derived conversion formulae allows a simple but consistent use in practical applications.

REFERENCES

- Bazant, Z.P. & Oh, B.H. 1983. Crack band theory for fracture of concrete. In: *Materials and Structures* 16, No. 93:155-177.
- Castro-Montero, A. & Jia, Z. & Shah, S.P. 1995. Evaluation of damage in brazilian test using holographic interferometry. In: *ACI Materials Journal* 92, No. 3: 268-275.
- CEB-FIP MC 90. 1993. COMITÉ EURO-INTERNATIONAL DU BÉTON: CEB-FIP Model Code 1990, Bulletin D'Information, No. 213/214. Lausanne: Thomas Telford Services Ltd.
- DIANA, 2007. Finite Element Analysis: User's Manuals release 9.2, TNO Building and Construction Research, Delft.
- DIN EN 12390. 2001. Prüfung von Festbeton. Berlin: Beuth.
- DIN 1048. 1991. Beuth Verlag GmbH.
- Hannant, D.J. & Buckley, K.J. & Croft, J. 1973. The effect of aggregate size on the use of the cylinder splitting test as a measure of tensile strength. In: *Materials and Structures* 6, No. 31: 15-21.
- Malárics, V. & Müller, H.S. 2007. Experimental and numerical analysis of the fracture process at the splitting tension test for concrete. In: *Proceedings of the 6th international conference on fracture mechanics of concrete and concrete structures*, Catania, Italy, 17-22 June 2007. Taylor & Francis/Balkema, Carpinteri, et al. (Eds.), pp. 225-232.
- Malárics, V. 2010. Ermittlung der Betonzugfestigkeit aus dem Spaltzugversuch bei festen und hochfesten Betonen. *Karlsruher Institut für Technologie, Institut für Massivbau und Baustofftechnologie*, Diss. (in preparation)
- Mechtcherine, V. 2000. Bruchmechanische und fraktologische Untersuchungen zur Rissausbreitung in Beton. *Universität Karlsruhe (TH), Institut für Massivbau und Baustofftechnologie*, Diss.
- RILEM CPC 7. 1975. Direct Tension. Final Recommendation. E & FN Spon.
- Tedesco, J.W. & Ross, C.A. & Kuennen, S.T. 1993. Experimental and numerical analysis of high strain rate splitting tensile tests. In: *ACI Materials Journal* 90, No. 2: 162-169.